Vibrational dynamics of the salicylideneaniline molecule in the solid phase and the confined state

Matthieu Hureau, Konstantin Smirnov, Alain Moissette, Hervé Jobic

Vibrational dynamics of the salicylideneaniline molecule in the solid phase and the confined state

Matthieu Hureau,[a] Konstantin S. Smirnov,*[a] Alain Moissette[a] and Hervé Jobic[b]

The salicylideneaniline (SA) molecule, both in the solid phase and sorbed in silicalite-1 zeolite, was studied by a large palette of vibrational spectroscopic methods (INS, Raman, and infrared) and by computational techniques. The comparison of the experimental and calculated spectra unambiguously indicates that the molecule is present in the *cis*-enol form in both phases. The results of the study allowed the proposal of a complete assignment of the vibrational spectrum of the SA molecule. The analysis of peak positions in the Raman and INS spectra of the molecule in the solid and sorbed states, and of the corresponding vibrational modes, shows that the confinement by the zeolite mostly affects those modes whose vibrational amplitude is localized on atoms of the phenol ring. This finding suggests that the molecule sits in the zeolite void such that the phenol ring is affected by the sorption to a greater extent than the benzene one. This assumption is corroborated by results of molecular modeling that shows the most energetically preferred position of the molecule in the straight channel of the zeolite framework with the phenol ring lying between two channel intersections, whereas the benzene ring is situated in the intersection.

1 Introduction

There has been a considerable interest over the last few decades in molecular compounds exhibiting photochromic properties, which are of crucial importance for the development of photosensible devices such as optical memories and photoswitches.[1–5] Among such molecules, 2-hydroxybenzylideneaniline (hereafter referred to as salicylideneaniline, SA) has been a subject of studies that started almost half a century ago.[6] The SA molecule belongs to the Shiff bases family and is often considered as a prototype molecule revealing reversible photoreactivity.

The SA molecule can exist in several tautomer forms, as shown in Fig. 1. The structure of SA in a solid phase has been investigated in a number of studies[7–9] and crystalline salicylideneaniline was found to have three polymorphic forms of which two are photochromic, whereas one form is thermochromic.[9] It is generally agreed that the ground state SA isomer is the *cis*-enol form (Fig. 1a) and that the reactivity of the molecule is related to the proton transfer that leads to the formation of the *cis*-keto structure (Fig. 1b) in the excited state.[6] The photochromism of the SA molecule and of its derivatives was suggested to result from the existence of the twisting angle between the phenol and benzene rings, in contrast to the thermochromic forms that have a planar structure.[6,9–12] This assumption found support in a recent study of SA-related compounds.[13]

Numerous experimental and theoretical studies have been undertaken to unravel the mechanism and rates of the elementary steps of SA photoreactivity, and to find out the intermediates along the reaction path.[14–21] Among different experimental techniques used to study photochromic molecules, methods of conventional vibrational spectroscopy provide the information at the length- and time-scale relevant to the process of interest. Despite the long history of studies on the photochromism of SA, vibrational spectroscopic investigations of the molecule in both the solid state and solution are few in number.[22–26] Most of these works were primarily focused on changes in the electronic spectrum of the molecule upon photoexcitation, whereas results obtained by means of vibrational spectroscopy were limited to specific spectral intervals, commonly the C=N mode region, around 1600 cm^{-1}. Furthermore, the assignments of bands to the vibrational modes of the molecule were incomplete.

Among the papers cited above, that by Turbeville and Dutta[24] reported the most comprehensive results. Making use of

[a] *Laboratoire de Spectrochimie Infrarouge et Raman, UMR 8516 CNRS et Université Lille 1 – Sciences et Technologies, 59655 Villeneuve d'Ascq, France. E-mail: Konstantin.Smirnov@univ-lille1.fr; Fax: +33 3 2043 6755; Tel: +33 3 20436139*

[b] *Institut de Recherches sur la Catalyse et l'Environnement de Lyon UMR-CNRS 5256, 2 avenue Albert Einstein, 69626 Villeurbanne, France*

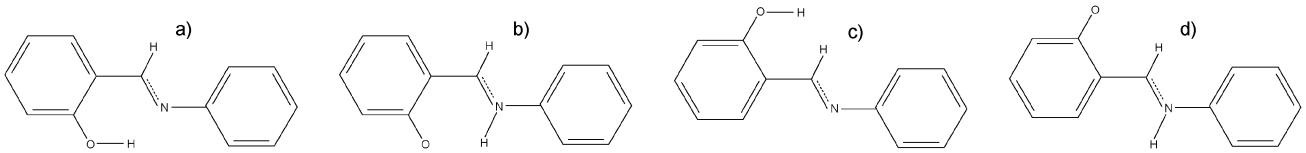

Fig. 1 Isomers of the salicylideneaniline molecule: *cis*-enol (a), *cis*-keto (b), *trans*-enol (c), and *trans*-keto (d).

resonance Raman, infrared, and NMR spectroscopy the authors investigated the characteristics of the SA molecule in a crystalline form, in different solutions, and sorbed in large cages of NaY zeolite. The observed spectral features in the region 1000 to 1700 cm^{-1} were classified into different groups and the assignment of bands was performed with the use of isotopic deuterium and ^{15}N substitution. The influence of the solvent nature on the spectra of the molecule was studied and the photoproduct of SA in the solid form was ascribed to the *trans*-keto SA isomer (*cf.* Fig. 1d).

The first goal pursued in the present work is to investigate the vibrational dynamics of the SA molecule in a solid phase with particular attention to covering whole spectral interval characteristics of molecular vibrations and on the assignment of observed spectral features to the vibrational modes. The second goal of the study is to characterize salicylideneaniline confined in an inorganic matrix. The reason for this second objective is that such a matrix (acting like a solvent) has a number of advantages over the classical fluid solvents because it provides a controlled geometrical and chemical environment, a degree of confinement, and a high thermal stability. Silicalite-1 zeolite (all-silica analog of ZSM-5 zeolite) is chosen in the present study as such a host medium.[27] This material is characterized by the smaller size of its pores and it is more chemically inert than the NaY zeolite used in previous works on SA–zeolite systems.[24,28] Because of the inert nature of silica walls and the fact that the size of zeolite pores tightly fits the size of the molecule, one can expect that SA sorbed in silicalite-1 should exist in an immobile quasi-isolated state.

These goals are achieved by using a number of experimental techniques such as the Raman, infrared, and inelastic neutron scattering (INS) spectroscopies. The complementary information obtained by these methods are supplemented by results of quantum-chemical calculations and molecular modeling. Such a combination of the methods allows us to report the most complete, to the best of our knowledge, vibrational spectroscopic study of the salicylideneaniline molecule in the condensed phase. For the sake of clarity and to keep the paper within a reasonable scope, no results concerning the electronic spectra of the molecule or the vibrational spectra of photochromic products are presented here. Furthermore, the high-frequency region of C–H, N–H, and O–H stretching vibrations is excluded from the discussion as it is less informative.

2 Experimental and computational procedures

2.1 Experimental part

Sample preparation. Salicylideneaniline was obtained from Sigma Aldrich (97%) in powder form that was used as is. Weighed amounts (*ca.* 1.2 g) of silicalite-1 were introduced into an evacuable and heatable glass cell placed in a vertical oven connected to a piping network. The sample was heated stepwise up to 450 °C under a flow of dry argon for 3 hours and then cooled to room temperature in the argon atmosphere. Amounts of salicylideneaniline corresponding to one molecule per two unit cells of silicalite-1 structure were introduced into the cell under a dry argon atmosphere and then the powder mixture was shaken. After a homogeneous mixing the powder was transferred in a quartz glass Suprasil cell under dry argon, sealed, and stocked at 40 °C. The process of sorption of the SA molecule into silicalite-1 was monitored by conventional diffuse reflectance UV-visible absorption spectroscopy and Raman spectroscopy. After six months, the UV-vis and Raman spectra of the system did not show any further evolution, thus indicating that the system had come to an equilibrium and that SA was present in the zeolite void in a molecular form.

The experimental protocol is identical to that used previously in the studies of anthracene,[29] *t*-stilbene,[30] and *N*-alkylphenothiazine[31] sorbed in ZSM-5 zeolites, where the molecules were found to penetrate the zeolite pore systems.

Raman measurements. Raman spectra of the SA molecule in a solid phase were measured with a HR Labram spectrometer using 632 nm laser radiation and a resolution of 0.3 cm^{-1}. The accumulation time was equal to 60 s and an average of 20 spectra was taken. The spectra of the molecule in a sorbed state were obtained either with the same setup and conditions indicated above, or by using a FT-Raman Bruker spectrometer with a 1064 nm excitation wavelength and 100 mW laser power. In the latter case the resolution was equal to 1 cm^{-1} and the spectra were averaged over 1600 scans.

DRIFT measurements. DRIFT spectra of SA in a solid phase were recorded by the ATR technique with a resolution of 2 cm^{-1}, and the spectra were averaged over 400 scans. The spectra of silicalite-1 and of the SA molecule sorbed in the zeolite were measured with a diffuse reflection sphere under flux of argon and at room temperature. The spectra were averaged over 1800 scans with a resolution of 2 cm^{-1} and the region between 1320 and 1400 cm^{-1} was omitted because the IR signal arising from the zeolite in this spectral region was too strong.

INS measurements. Inelastic neutron scattering experiments were carried out using the new spectrometer LAGRANGE at the Institut Laue-Langevin, Grenoble, France. This spectrometer combines an extended energy range, a higher resolution, and an increased detected flux compared with the previous instrument. The scattering cross-section for hydrogen being much larger than of other elements, INS traditionally emphasizes vibrational modes involving hydrogen atoms. In this work, measurements were

performed using a Cu(220) monochromator. The estimated accuracy on the frequency values is ± 10 cm^{-1}.

The samples were transferred inside a glovebox, into cylindrical aluminum cells. The cells were placed in a cryostat and cooled to 10 K to decrease the influence of the Debye–Waller factor, and thus sharpen peaks in the vibrational spectra.

2.2 Computational part

Quantum-chemical calculations. The calculations employed density functional theory and were performed at the B3LYP level with the 6-311++G(d,p) basis set. The hybrid B3LYP exchange–correlation (XC) functional is known to be reliable for computing the vibrational spectra of both isolated and periodic systems.[32,33] This combination of the XC functional and basis set was successfully used in our previous study of *trans*-stilbene sorbed in ZSM-5 zeolites.[34] Structures of different isomers of the enol and keto forms of the salicylideneaniline molecule were optimized in the C_1 and C_S point symmetry groups. As soon as the stationary point was found, the structural optimization was followed by a vibrational analysis, indicating whether the optimized structure corresponded to a minimum or to a saddle point on the potential energy surface. The calculations were done with the Gaussian 09 code.[35]

Spectra calculations. The computation of the infrared and Raman activities of the vibrational modes of the SA isomers was carried out by using the internal capabilities of the Gaussian 09 program. The Raman scattering intensity I_m of mode m with the angular frequency ω_m was subsequently obtained as

$$I_m = \frac{(\omega_0 - \omega_m)^4}{\omega_m(1 - \exp(-\hbar\omega_m/k_B T))} R_m, \qquad (1)$$

where ω_0 is the frequency of the incident radiation, T is the temperature, and $\hbar$ and k_B have their conventional meaning. The quantity R_m is the Raman activity computed under the assumption of linearly polarized incident radiation. As the peak intensities in the DRIFT and IR absorbance spectra have no one-to-one correspondence, computed values of the IR absorption coefficients were used for a semi-quantitative analysis of the data of the DRIFT measurements. The resulting Raman and IR stick spectra were convoluted with a Lorentzian function with HWHM = 2 cm^{-1}.

The inelastic neutron-scattering spectra were simulated by using an approach described elsewhere.[34,36–39] The calculations were carried out both in the isolated molecule approximation and considering the contribution of bath phonons to the scattering intensity. In the latter case the phonon bath frequency was taken to be equal to 100 cm^{-1}; a reason for choosing this value of the bath mode is discussed below. The resulting stick spectra were convoluted with a Gaussian function whose width parameter σ mimicked the resolution function of the LAGRANGE spectrometer.

As the quantum-chemical calculations generally overestimate the frequencies of vibrational modes, corrected frequency values ω_{sc} were obtained with the help of scaling function

$$\omega_{sc} = a\omega_{QC} + b, \qquad (2)$$

where ω_{QC} is the frequency obtained in the quantum-chemical calculations, and the parameters a = 0.9724 and b = 6.7 cm^{-1} were found by a linear least squares regression of theoretical *vs.* experimental frequencies of the *trans*-stilbene molecule in the region 0–1700 cm^{-1}.[34] Note that the parameter values in eqn (2) are by no means universal and are bounded by the combination of XC functional/basis set. In the following discussion, the frequency values refer to the scaled theoretical frequencies ω_{sc}, if not explicitly stated otherwise.

Molecular modeling. The simulation of the sorption position of the SA molecule in the MFI structure was carried out by using a combination of Monte-Carlo and energy minimization techniques. The simulations were performed with the Materials Studio program suite.[40] The model system consisted of two unit cells ($1 \times 1 \times 2$) of the orthorhombic silicalite-1 lattice (576 atoms) and one sorbed SA molecule. The zeolite framework was assumed to be rigid. The interaction of the molecule with the atoms of the host lattice was described as the sum of electrostatic and van der Waals interaction potentials. The partial atomic charges of atoms of the SA molecule were computed with the electronegativity equalization method using parameters reported in ref. 41, set T1. Charges of magnitude +1.36 $|e^-|$ and -0.68 $|e^-|$ were assigned to the silicon and oxygen atoms of the zeolite lattice, respectively. These values are the mean values of ESP charges computed by the split-charge equilibration method with parameters given in ref. 42. Test calculations have revealed that the electrostatic energy gives a minor contribution to the host–guest interaction energy that is dominated by the van der Waals interactions.

To choose the van der Waals interaction potential, a number of force fields were tested against experimental values of the heat of adsorption H_{ads} of benzene and phenol molecules in silicalite-1, that can be viewed as constituent blocks of the SA molecule. These test calculations have shown that the reference values are best reproduced with the combination of the above charge parameters and the PCFF force field.[43] Thus, the calculated heat of adsorption of benzene in silicalite-1 is equal to H_{ads} = 54.7 kJ mol^{-1} and is in a good agreement with the experimental values of 52 kJ mol^{-1} and 50 kJ mol^{-1} by Pope[44] and by Song and co-workers,[45] respectively. The computed value of the heat of adsorption of phenol in silicalite-1 H_{ads} = 65.9 kJ mol^{-1} is in good agreement with a theoretical estimation of 61.7 kJ mol^{-1} obtained by Klemm *et al.*[46] The intramolecular interactions in the SA molecule were also described with the use of the PCFF force field.[43]

The host–guest interaction energy E_{hg} was computed as $E_{hg} = E_T - E_h - E_g$, where E_T, E_h and E_g are the total energy of the system, the energy of the zeolite framework, and the intramolecular energy, respectively. The latter quantity was calculated by taking the geometry of the molecule in the confined state.

3 Results and discussion

3.1 Relative stability of SA isomers

Table 1 reports the relative energies of the SA molecule isomers computed at the B3LYP/6-311++(d,p) level with respect to the lowest energy structure. Results of the DFT calculations show

Table 1 Relative energies of SA isomers (*cf.* Fig. 1)

Isomer	Relative energy/kJ mol^{-1}
cis-Enol form	0.00
cis-Enol form 2[a]	55.23
trans-Enol form	45.40
trans-Enol form 2[a]	38.58
cis-Keto form	19.50
trans-Keto form	61.92

[a] Proton of OH group in *trans* position.

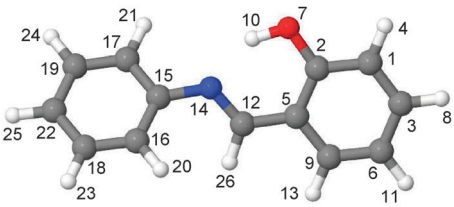

Fig. 2 *cis*-Enol form of the SA molecule. Light gray, gray, red, and blue balls correspond to hydrogen, carbon, oxygen, and nitrogen atoms, respectively.

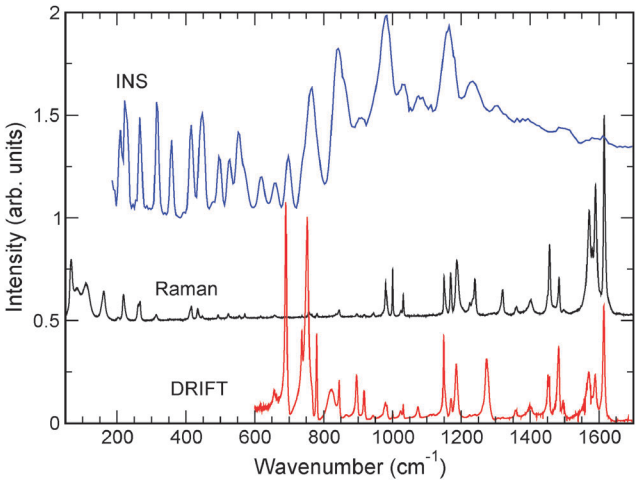

Fig. 3 Experimental vibrational spectra of the SA powder sample.

that the *cis*-enol form (Fig. 2) is the most stable conformer and this form is more energetically preferred than the *cis*-keto isomer, by 19.5 kJ mol^{-1}. All other conformers have energies lying 38 to 62 kJ mol^{-1} higher than that of the *cis*-enol SA isomer. For each conformer the structure optimization in the C_S symmetry resulted in an energy value very close to that obtained in the optimization without the symmetry constraint. However, these planar structures with the C_S symmetry were found to have a negative frequency corresponding to twisting the benzene and phenol rings with respect to each other. The resulting C_1 structure of the *cis*-enol SA isomer has a twisting angle of 38.2°. The energy difference between the SA conformers and the structural parameters of the most stable *cis*-enol form of the molecule obtained in the present work are in good agreement with results of recent computational studies performed with basis sets of similar quality.[19,21] The computed value of the twisting angle between the rings is, however, notably smaller than the values obtained experimentally in refs. 7–9. A credible explanation for this difference is that the calculations were carried out for a free molecule, whereas the experimental angle values were obtained for molecules in crystalline samples of the two α polymorphs of SA. The calculations show that the potential energy surface along the twisting angle coordinate is very flat. Thus, the mode frequency is $\omega_{QC} = -46$ cm^{-1} and the energy difference between the planar C_S and twisted C_1 SA structures is only 3.94 kJ mol^{-1}, *i.e.* $\approx 1.6\ k_BT$ at the ambient temperature. The corresponding values reported by Ortiz-Sánchez *et al.*[19] are −47 cm^{-1} and 3.14 kJ mol^{-1}.

3.2 Vibrational spectra of SA in the solid phase

Fig. 3 shows the vibrational spectra of SA powder recorded with the three spectroscopic techniques. The complementary nature of the methods permits a detailed analysis of the observed spectral features. The Raman spectroscopy provides the most pertinent data because it covers the entire frequency interval of interest. Nevertheless, in the spectral region below 900 cm^{-1}, where the Raman scattering has a low intensity, the INS spectroscopy yields a wealth of information amplified by the high resolution of the LAGRANGE spectrometer in this region.[47] The DRIFT spectrum completes the characterization.

Fig. 4 and 5 compare the experimental Raman and INS spectra of the SA powder with the corresponding spectra calculated for the two most stable forms of the SA molecule: the *cis*-enol and *cis*-keto isomers. The analysis of these figures unambiguously indicates that the molecule in the solid phase exists in the *cis*-enol form. A slight difference in the position of peaks and/or intensities of some modes can be ascribed to a systematic error inherent to the theoretical level used in the calculations, and to the fact that the calculations were performed for an isolated molecule.

Making use of the results of the calculations and the analysis of the intensities in the Raman, IR, and INS spectra, one can suggest a complete assignment of the observed spectral features to the vibrational modes of the molecule.† It is noteworthy that due to lowering the resolution in the INS spectra,[47] the spectral features above 600 cm^{-1} are the envelopes of several vibrational modes that hamper a precise attribution of the INS peaks in this energy region. However, the complementary nature of the three spectroscopic techniques facilitates the removal of uncertainties in the attribution.

The suggested assignment† completes that by Turbeville and Dutta[24] and, in some cases, corrects their attribution of observed Raman peaks to specific modes. Thus, the calculations unambiguously reveal that the experimental Raman peaks at 1590 cm^{-1} and 1484 cm^{-1} can be characterized as modes of the benzene ring, and not the phenol ring (there is a systematic shift of *ca.* 6 cm^{-1} between the mode frequencies measured in the present work and the values reported in ref. 24). The most important contributions to the potential energy distribution (PED) of these two modes come from the internal coordinates formed by the atoms of the former entity. Fig. 6 displays the vibrational mode with $\omega_{sc} = 1185$ cm^{-1} that was ascribed to a mixed C–O stretching and O–H bending vibration.[24] The calculations show

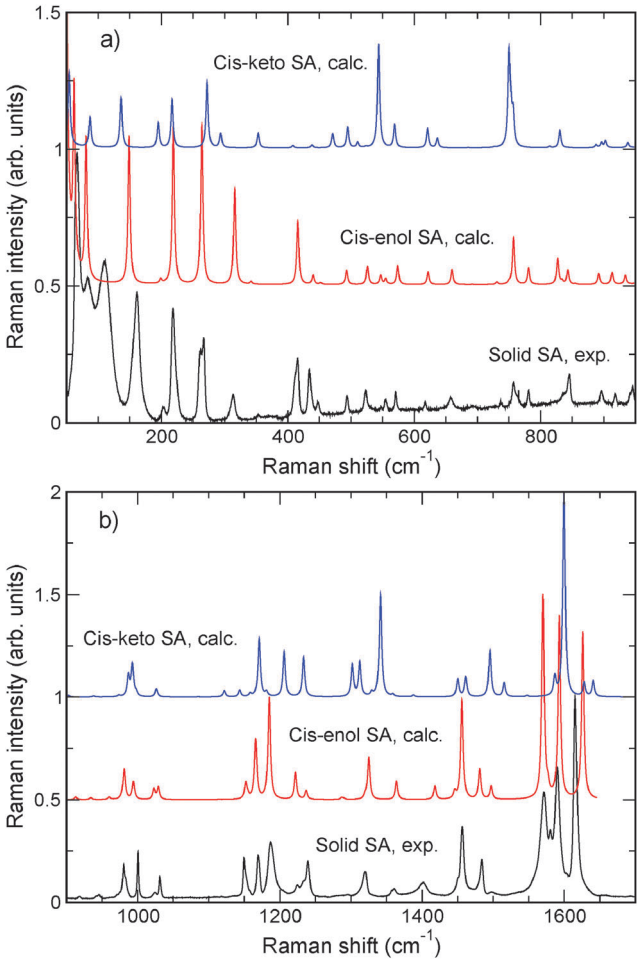

Fig. 4 Low- (a) and mid-frequency (b) parts of the experimental Raman spectrum of SA powder and of the calculated Raman spectra of the two most stable SA isomers.

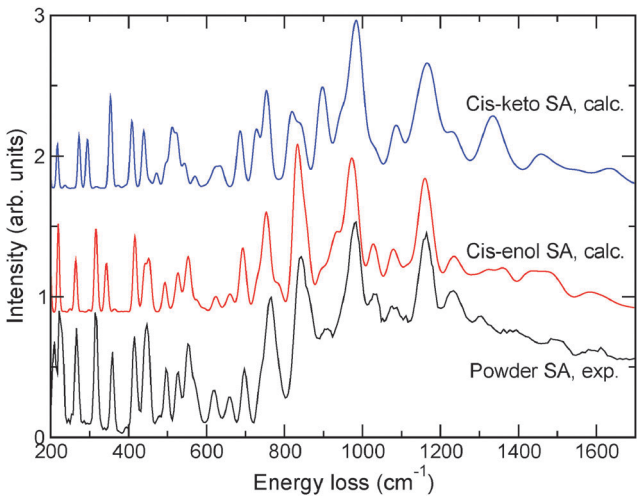

Fig. 5 Experimental INS spectrum of SA powder and the calculated INS spectra of the two most stable SA isomers.

that the most important contributions to PED of the mode actually come from the C15–N14 and C12–C5 bond stretching,

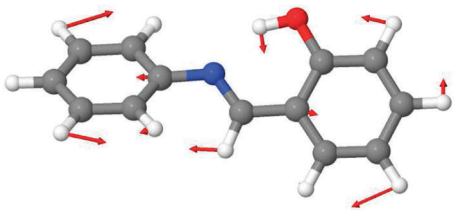

Fig. 6 Displacements of atoms in the vibrational mode with ω_{sc} = 1185 cm^{-1}. The vibrational amplitudes were scaled by a factor of 5.

73% and 48%, respectively, whereas the contribution of the C2–O7 stretching and C2–O7–H10 bending internal coordinates is only 13% and 1%, respectively (*cf.* Fig. 2 for atom numbering). The interested reader is referred to Table S1 of ESI† for more details on the mode assignment.

The experimental Raman spectrum of the SA molecule in the solid state contains one peak at 111 cm^{-1} that cannot be assigned on the basis of the calculations. Supplementary measurements have shown that the peak position is sensitive to temperature. Thus, the peak shifts to 120 cm^{-1} when the temperature is lowered to 123 K. Furthermore, anticipating results presented in the following section, the peak is absent in the Raman spectrum of the SA molecule sorbed in silicalite-1. Taking these facts into account, the peak at 111 cm^{-1} is attributed to an intermolecular mode of the SA molecules in the solid phase. The intermolecular mode frequency *a posteriori* justifies the frequency value of the bath mode used in the INS spectra modeling.

3.3 Vibrational spectra of the sorbed SA molecule

Silicalite-1 has the MFI structure type and its framework is characterized by a porous system consisting of intersecting channels formed by rings of ten oxygen atoms.[27] Straight channels run along the *b* crystallographic axis and have a nearly circular shape with dimensions of 5.3 Å × 5.6 Å, while a second type of channel, termed sinusoidal channels, have an average direction along the *a* axis with dimensions of 5.1 Å × 5.5 Å. The diameter of a sphere that can diffuse along the *a*- and *b*-directions is equal to 4.7 and 4.46 Å, respectively.[27] These values are very close to the transverse size of the SA molecule estimated as 4.6 Å. The distance between the channel intersections is *ca.* 10 Å that is slightly smaller than the length of the SA molecule (*ca.* 11.4 Å).

Fig. 7 presents the Raman and INS spectra of the SA molecule sorbed in silicalite-1 and compares the spectra with those of the molecule in solid phase. A relatively low resolution in the INS spectra above 600 cm^{-1} and the proximity of some vibrational modes hamper the detailed interpretation of the spectrum variation in this spectral region. Nevertheless, the combination of the INS and Raman scattering techniques allows us to extract the maximum information from the comparison. Unfortunately, the infrared spectrum is dominated by the diffuse reflectance signal due to the zeolite lattice, and therefore the spectrum is useless for a quantitative analysis.

The analysis of the spectra in Fig. 7 shows that the Raman and INS spectra of the molecule in the solid and sorbed states

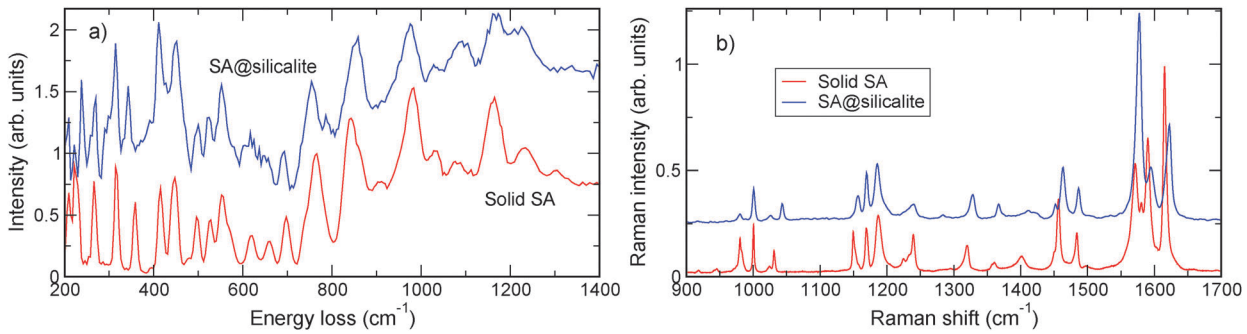

Fig. 7 INS (a) and Raman (b) spectra of the SA molecules sorbed in silicalite-1 (noted hereafter as SA@silicalite) compared with the spectra of the molecule in solid phase.

Table 2 Vibrational modes of the *cis*-enol SA molecule with maximum frequency shift upon sorption. Potential energy distribution (PED) reports internal coordinates and the corresponding percentage (in parentheses) of three largest contributions to the PED for each mode. Internal coordinates definition: R – bond-stretching, δ – angle-bending, ω – out-of-plane, τ – torsion; numbering of atoms corresponds to Fig. 2. D_m^P, D_m^B, and D_m^I stand for the amplitude localization criterion (3) for the phenol, benzene rings, and imine group, respectively

ω_{exp}/cm^{-1}							
Solid SA	SA@silicalite	$\Delta\omega$	ω_{sc}/cm^{-1}	PED	D_m^P/%	D_m^B/%	D_m^I/%
161	152	−9	149	τ_{C2C5} (93), τ_{C5C9} (26), τ_{O2H7} (22)	48.8	43.7	7.5
218	231	+13	219	τ_{C2C5} (89), τ_{C1C2} (37), τ_{C5C12} (19)	56.6	6.0	37.4
360	342	−18	342	τ_{C5C9} (78), τ_{C1C3} (34), ω_{C1H4} (26)	45.9	29.1	25.0
1031	1043	+12	1029	R_{C3C6} (91), R_{C1C3} (28), R_{C9C6} (18)	96.2	3.6	0.2
1149	1157	+8	1152	$\delta_{C3C6H11}$ (44), $\delta_{C9C6H11}$ (42), δ_{C6C3H8} (41)	98.0	1.4	0.6
1273	1283	+10	1287	R_{C2O7} (94), δ_{C1C3H8} (15), R_{C5C12} (15)	78.7	8.2	13.2
1319	1328	+9	1325	R_{C2C5} (63), R_{C1C3} (43), R_{C9C6} (42)	64.2	32.4	3.3
1401	1411	+10	1418	$\delta_{C2O7H10}$ (90), R_{C1C3} (23), R_{C5C9} (16)	97.6	0.2	2.2
1456	1463	+7	1456	R_{C2O7} (50), R_{C2C5} (49), R_{C9C6} (41)	89.8	7.0	3.2
1571	1577	+6	1570	R_{C12N14} (57), $\delta_{C2O7H10}$ (53), R_{C1C3} (39)	85.2	7.1	7.7

are very similar to each other. It is, however, instructive to analyse those vibrational modes of the SA molecule whose frequencies are affected by the sorption to the maximum extent. These modes are listed in Table 2. The comparison of the frequencies of the vibrational modes of the molecule in the solid and sorbed states shows that the frequency differences are relatively small and the maximum difference does not exceed 18 cm^{-1}. Such a small frequency shift points to a weak perturbation of the molecule by the sorption and indicates that silicalite-1 is a relatively inert environment. It is worthy to note that the Raman spectrum of the sorbed molecules does not contain the peak at 111 cm^{-1}, which supports the assignment of this peak to an intermolecular mode.

Table 2 shows that the two modes with frequencies ω_{sc} = 149 and 342 cm^{-1} undergo a downward frequency shift upon sorption. Analysis of the atomic displacements reveals that these modes have a similar form that can be described as the anti-phase motion of the phenol and benzene rings in the direction perpendicular to the plane of the rings. A possible explanation for the downward shift of their vibrational frequencies is that the intermolecular interactions in the solid phase constrains these vibrations to a larger extent than the interactions with the silicalite-1 lattice. This hypothesis is in line with the disappearance of the peak at 111 cm^{-1} in the Raman spectrum of sorbed salicylideneaniline.

Most of the modes represented in Table 2 are shifted upward upon sorption. Analysis of the potential energy distribution in the modes shows that the dominant contributions to PED come from the internal coordinates of the phenol ring. Thus, the mode with ω_{sc} = 1029 cm^{-1} (Table 2) with a frequency shift of +12 cm^{-1} upon sorption has 91% of the potential energy coming from the variation of the C3–C6 bond. The atomic displacements in the mode are shown in Fig. 8a, which illustrates that the vibrational amplitude is localized on the light hydrogen atoms of the phenol ring.

Therefore it is of interest to analyse the atomic displacements and their localization in the modes that are shifted upon sorption.

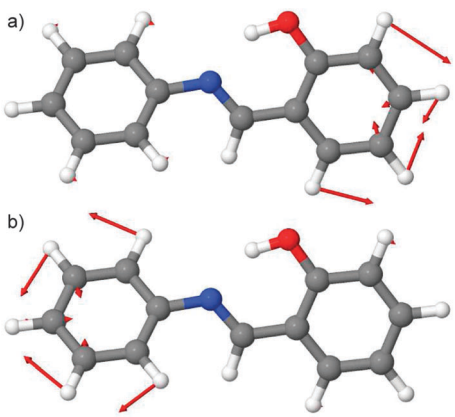

Fig. 8 Displacements of atoms in the vibrational modes with ω_{sc} = 1029 cm^{-1} (a) and ω_{sc} = 1023 cm^{-1} (b) (*cf.* caption to Fig. 6).

For this purpose three groups of atoms were defined in the molecule: atoms of the phenol ring, the benzene ring, and those of the imine group. The degree of localization D_k^m for atoms of group k in mode m was calculated as

$$D_k^m = \sum_{i \in k} \left(\mathbf{L}_x^{im}\right)^2 \Big/ \sum \left(\mathbf{L}_x^{im}\right)^2, \qquad (3)$$

where $\mathbf{L}_x^{im}$ stands for the vector of Cartesian displacements of atom i in the mode m; the sum in denominator runs over all atoms of the molecule. Values of the D_k^m criteria are reported in the right-hand part of Table 2. The analysis of the values shows that the vibrational amplitude of almost all modes with a large upward frequency shift is localized on the phenol ring. Thus, 96% of the vibrational amplitude of the mode with ω_{sc} = 1029 cm^{-1} is due to the displacements of H atoms of the phenol ring (Fig. 8a). For comparison, the mode with ω_{sc} = 1023 cm^{-1} (Fig. 8b) in which displacements of atoms are similar to those in the ω_{sc} = 1029 cm^{-1} mode, but the amplitude is localized on the atoms of benzene ring (D_m^B = 97.5%), undergoes a frequency shift of only +2 cm^{-1}. It should, however, be noted that the trend is not universal and, for example, the mode with ω_{sc} = 1325 cm^{-1} is shifted by +9 cm^{-1}, while it has comparable D_m^k values for both the phenol and benzene rings.

In our opinion, such different behaviours of the vibrational mode frequencies reflects a different degree of confinement of the phenol and benzene rings of the molecule by the silicalite-1 framework. Indeed, large frequency shifts of the modes localized on the phenol ring indicate that this part of the sorbed molecule is more constrained than the benzene ring. Given the size and shape of the molecule and the topology of the zeolite void, one can suggest that the benzene ring of SA resides in the intersection of the straight and sinusoidal channels, whereas the phenol ring is situated in the section of the straight channel between two intersections, where the ring is subjected to a larger confinement than the benzene one. From the structural view-point it is unlikely that the molecule can reside in a sinusoidal channel because the topology of the zeolite pore system would apply too strong constraints on the molecular geometry. Consequently, we propose that the most probable adsorption site of the SA molecule is the straight channels of the silicalite-1 framework. This assumption is supported by results of molecular modeling.

Fig. 9 displays the position of the SA molecule inside the zeolite framework in the most energetically favored sorption site, after the energy minimization procedure. The molecule lies in the straight channel with the benzene ring situated in the channel intersection, as it was deduced from the analysis of the vibrational frequency shifts. The host–guest interaction energy E_{hg} in this sorption site is E_{hg} = −113.6 kJ mol^{-1}. The calculation of the E_{hg} energy profile of the SA molecule along a straight channel reveals that this sorption position is *ca.* 8 kJ mol^{-1} more energetically preferred than a position with the phenol ring lying in the intersection (E_{hg} = −105.8 kJ mol^{-1}). Our test simulations of the phenol sorption in silicalite-1 have shown that the molecule prefers a position in a channel intersection with the OH group pointing to sinusoidal channel. Such an orientation of the phenol ring of sorbed SA molecule would, however, cause too strong structural distortions of the molecule and thus is energetically unfavored. Forcing the SA molecule to be sorbed in a sinusoidal channel has resulted in a E_{hg} energy of *ca.* −34 kJ mol^{-1}, that is much higher than the host–guest interaction energy for the molecule sorbed in the straight channel.

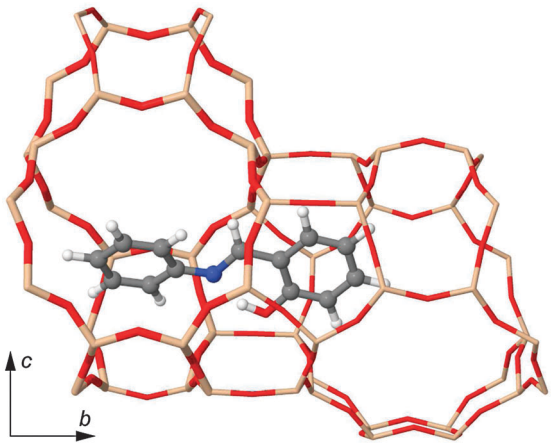

Fig. 9 A view of the SA molecule sorbed in silicalite-1. A piece of zeolite framework between two intersections of straight and sinusoidal channels is shown. The straight channel runs along the *b*-axis, the sinusoidal channels have an average direction perpendicular to the image plane (*a*-axis). The intersection of the straight and sinusoidal channels, where the benzene ring is situated, is highlighted with bold sticks.

4 Conclusions

The vibrational spectra of the salicylideneaniline (SA) molecule in the solid phase and confined in silicalite-1 zeolite were studied using a large palette of vibrational spectroscopic methods in addition to computational techniques. The comparison of Raman, infrared, and inelastic neutron scattering spectra of the SA molecule with the theoretical spectra obtained by using results of quantum-chemical calculations of different SA isomers in a free state, unambiguously shows that the molecule exists in the *cis*-enol form in a condensed phase. The analysis of the experimental data is greatly facilitated by the complementary nature of the techniques and by the comparison of the experimental and calculated peak intensities. Making use of the results of the calculations, a complete assignment of the observed spectral features to the vibrational modes of the molecule is performed.

All experimental spectroscopic data indicate that the sorbed SA molecules are present in the *cis*-enol form in the zeolite channels. The confinement induces only a weak perturbation of the vibrational dynamics of the molecule in comparison with that in solid SA. The displacements of spectral peaks in the Raman and INS spectra of SA upon sorption and the analysis of the corresponding vibrational modes show that the confinement mostly affects the vibrational modes whose amplitude is

localized on atoms of the phenol ring. This finding allows the suggestion that the sorbed SA molecule is located in the zeolite channel, such that the phenol ring lies in the section of the straight channel between two intersections, whereas the benzene ring is situated at the channel intersection. This assumption is corroborated by results of molecular modeling using a combination of Monte-Carlo and energy minimization techniques.

Acknowledgements

The neutron measurements were performed on the LAGRANGE spectrometer at the Institut Laue-Langevin, Grenoble, France. The authors are grateful to Dr M. Jimenez-Ruiz for her help during the experiments.

References

1 M. Irie, *Chem. Rev.*, 2000, **100**, 1683–1684.
2 M. Irie, *Chem. Rev.*, 2000, **100**, 1685–1716.
3 Y. Yokoyama, *Chem. Rev.*, 2000, **100**, 1717–1740.
4 G. Berkovic, V. Krongauz and V. Weiss, *Chem. Rev.*, 2000, **100**, 1741–1754.
5 S. Kawata and Y. Kawata, *Chem. Rev.*, 2000, **100**, 1777–1788.
6 M. D. Cohen and G. M. J. Schmidt, *J. Phys. Chem.*, 1962, **66**, 2442–2446.
7 R. Destro, A. Gavezzotti and M. Simonetta, *Acta Crystallogr., Sect. B: Struct. Crystallogr. Cryst. Chem.*, 1978, **34**, 2867–2869.
8 F. Arod, M. Gardon, P. Pattison and G. Chapuis, *Acta Crystallogr., Sect. C: Cryst. Struct. Commun.*, 2005, **61**, o317–o320.
9 F. Arod, P. Pattison, K. J. Schenk and G. Chapuis, *Cryst. Growth Des.*, 2007, **7**, 1679–1685.
10 M. D. Cohen, G. M. J. Schmidt and S. Flavian, *J. Chem. Soc.*, 1964, 2041–2051.
11 J. Bregman, L. Leiserowitz and K. Osaki, *J. Chem. Soc.*, 1964, 2086–2100.
12 I. Moustakali-Mavridis, E. Hadjoudis and A. Mavridis, *Acta Crystallogr., Sect. B: Struct. Crystallogr. Cryst. Chem.*, 1978, **34**, 3709–3715.
13 K. Johmoto, T. Ishida, A. Sekine, H. Uekusa and Y. Ohashi, *Acta Crystallogr., Sect. B: Struct. Sci.*, 2012, **68**, 297–304.
14 S. Mitra and N. Tamai, *Chem. Phys.*, 1999, **246**, 463–475.
15 S. Mitra and N. Tamai, *Phys. Chem. Chem. Phys.*, 2003, **5**, 4647–4652.
16 M. Ziolek, J. Kubicki, A. Maciejewski, R. Naskrecki and A. Grabowska, *Phys. Chem. Chem. Phys.*, 2004, **6**, 4682–4689.
17 M. Sliwa, N. Mouton, C. Ruckebusch, L. Poisson, A. Idrissi, S. Aloise, L. Potier, J. Dubois, O. Poizat and G. Buntinx, *Photochem. Photobiol. Sci.*, 2010, **9**, 661–669.
18 M. Z. Zgierski and A. Grabowska, *J. Chem. Phys.*, 2000, **112**, 6329–6337.
19 J. M. Ortiz-Sánchez, R. Gelabert, M. Moreno and J. M. Lluch, *J. Chem. Phys.*, 2008, **129**, 214308.
20 B. Chowdhury, R. De, P. Sett and J. Chowdhury, *J. Chem. Sci.*, 2010, **122**, 857–865.
21 L. Spörkel, G. Cui and W. Thiel, *J. Phys. Chem. A*, 2013, **117**, 4574–4583.
22 J. W. Ledbetter, *J. Phys. Chem.*, 1968, **72**, 4111–4115.
23 J. W. Ledbetter, *J. Phys. Chem.*, 1982, **86**, 2449–2451.
24 W. Turbeville and P. K. Dutta, *J. Phys. Chem.*, 1990, **94**, 4060–4066.
25 D. Gegiou, E. Lambi and E. Hadjoudis, *J. Phys. Chem.*, 1996, **100**, 17762–17765.
26 L. R. Knöpke, A. Spannenberg, A. Brückner and U. Bentrup, *Spectrochim. Acta, Part A*, 2012, **95**, 18–24.
27 http://www.iza-structure.org/databases/.
28 I. Casades, M. Álvaro, H. García and M. Pillai, *Eur. J. Org. Chem.*, 2002, 2074–2079.
29 A. Moissette, S. Marquis, I. Gener and C. Bremard, *Phys. Chem. Chem. Phys.*, 2002, **4**, 5690–5696.
30 M. Hureau, A. Moissette, A. Legrand, F. Luchez, M. Sliwa and C. Bremard, *J. Phys. Chem. C*, 2012, **116**, 9092–9105.
31 S. Carré, F. Luchez, A. Moissette, O. Poizat and I. Batonneau-Gener, *ChemPhysChem*, 2012, **13**, 504–513.
32 A. P. Scott and L. Radom, *J. Phys. Chem.*, 1996, **100**, 16502–16513.
33 M. De La Pierre, R. Orlando, L. Maschio, K. Doll, P. Ugliengo and R. Dovesi, *J. Comput. Chem.*, 2011, **32**, 1775–1784.
34 M. Hureau, A. Moissette, K. S. Smirnov and H. Jobic, *J. Phys. Chem. C*, 2012, **116**, 15510–15518.
35 M. J. Frisch, G. W. Trucks, H. B. Schlegel, G. E. Scuseria, M. A. Robb, J. R. Cheeseman, G. Scalmani, V. Barone, B. Mennucci, G. A. Petersson, H. Nakatsuji, M. Caricato, X. Li, H. P. Hratchian, A. F. Izmaylov, J. Bloino, G. Zheng, J. L. Sonnenberg, M. Hada, M. Ehara, K. Toyota, R. Fukuda, J. Hasegawa, M. Ishida, T. Nakajima, Y. Honda, O. Kitao, H. Nakai, T. Vreven, J. A. Montgomery Jr., J. E. Peralta, F. Ogliaro, M. Bearpark, J. J. Heyd, E. Brothers, K. N. Kudin, V. N. Staroverov, R. Kobayashi, J. Normand, K. Raghavachari, A. Rendell, J. C. Burant, S. S. Iyengar, J. Tomasi, M. Cossi, N. Rega, J. M. Millam, M. Klene, J. E. Knox, J. B. Cross, V. Bakken, C. Adamo, J. Jaramillo, R. Gomperts, R. E. Stratmann, O. Yazyev, A. J. Austin, R. Cammi, C. Pomelli, J. W. Ochterski, R. L. Martin, K. Morokuma, V. G. Zakrzewski, G. A. Voth, P. Salvador, J. J. Dannenberg, S. Dapprich, A. D. Daniels, Ö. Farkas, J. B. Foresman, J. V. Ortiz, J. Cioslowski and D. J. Fox, *Gaussian 09 Revision B.01*, Gaussian Inc., Wallingford, CT, 2010.
36 H. Jobic, R. E. Ghosh and A. Renouprez, *J. Chem. Phys.*, 1981, **75**, 4025–4030.
37 H. Jobic and H. J. Lauter, *J. Chem. Phys.*, 1988, **88**, 5450–5456.
38 J. Tomkinson and G. J. Kearley, *J. Chem. Phys.*, 1989, **91**, 5164–5169.
39 J. Tomkinson and G. Kearley, *Nucl. Instrum. Methods Phys. Res., Sect. A*, 1995, **354**, 169–170.
40 *Materials Studio 6.1.0*, Accelrys Software Inc., San Diego, CA, 2012.
41 T. Verstraelen, P. Bultinck, V. Van Speybroeck, P. W. Ayers, D. Van Neck and M. Waroquier, *J. Chem. Theory Comput.*, 2011, **7**, 1750–1764.

42 T. Verstraelen, S. V. Sukhomlinov, V. Van Speybroeck, M. Waroquier and K. S. Smirnov, *J. Phys. Chem. C*, 2012, **116**, 490–504.
43 H. Sun, S. J. Mumby, J. R. Maple and A. T. Hagler, *J. Am. Chem. Soc.*, 1994, **116**, 2978–2987.
44 C. G. Pope, *J. Phys. Chem.*, 1986, **90**, 835–837.
45 L. Song, Z.-L. Sun, H.-Y. Ban, M. Dai and L. V. Rees, *Adsorption*, 2005, **11**, 325–339.
46 E. Klemm, J. Wang and G. Emig, *Microporous Mesoporous Mater.*, 1998, **26**, 11–21.
47 The FWHM of the LAGRANGE resolution function varies from 5 cm^{-1} at 120 cm^{-1} to 40 cm^{-1} at 1200 cm^{-1}.